A flow velocity dependence of dynamic surface tension in Plateau borders of foam

Clarke, Christopher; Spyropoulos, Fotis; Norton, Ian T.

DOI:
10.1016/j.jcis.2020.04.028

Document Version
Peer reviewed version

Citation for published version (Harvard):
Clarke, C, Spyropoulos, F & Norton, IT 2020, 'A flow velocity dependence of dynamic surface tension in Plateau borders of foam', *Journal of Colloid and Interface Science*, vol. 573, pp. 348-359.
https://doi.org/10.1016/j.jcis.2020.04.028

A Flow Velocity Dependence of Dynamic Surface Tension in Plateau Borders of Foam

Christopher Clarke, Fotis Spyropoulos and Ian T. Norton*

*Department of Chemical Engineering, University of Birmingham, Edgbaston, Birmingham, B15 2TT, UK

Abstract

Hypothesis

Liquid drainage through foams is a multiscale process, that primarily occurs through channels known as Plateau borders (PBs). Recent experimental studies of isolated PBs have observed variations in channel surface tension, γ, with liquid flow rate, Q, for systems containing soluble low molecular weight surfactant (LMWS). The current study proposes that the dynamic surface tension (DST) could be responsible for this effect, where the residence time of surfactant molecules in the PB is similar to the time required for their adsorption to the channel interface.

Experiments

Profile geometries of isolated 'ideal' PB's were created in a bespoke experimental setup at controlled forced liquid flow rates. Average surfactant residence times, τ_{Res}, were calculated for solutions of Sodium dodecylsulfate (SDS), Tween 20 (T20) and Tween 80 (T80), and used to calculate corresponding average DST values in discrete regions of measured PB profiles. DST values were combined with microscale drainage theory to assess the potential physical implications on liquid flow.

Findings

Significant variations in the magnitude of γ were calculated based on surfactant characteristics, where only the rapid adsorption of SDS was sufficient to produce DST values approaching equilibrium. These findings seriously question assumptions of near equilibrium surface tension in LMWS foam systems above their critical micelle concentration (CMC). Furthermore, the presence of surface tension gradients identified using this discrete approach, highlights the need to further refine the current theory to a continuous approach incorporating Marangoni effects.

Introduction

Background

Foam drainage is a highly complex phenomenon that is the combined result of dynamic processes occurring over a range of different length-scales[1]. Because of its essential role in destabilising foams, those seeking foam longevity often aim to retard this process, typically employing basic assumptions regarding liquid flow to inform a trial and error approach to formulation development[2]. While this tactic has been met with measured success, the increasing demand for foams with specific functionality, using a limited range of ingredients, has necessitated a much more rigorous approach to understanding foam microstructure and its impact on microscale liquid flow[3]; which in turn drives macroscopic behaviour.

At the microscale, liquid transport through foams primarily occurs through the interconnected network of channels between bubbles, known as Plateau Borders (PBs), and their junctions, or Nodes[4,5]. As these structures ultimately form the 'building blocks' of macroscopic foams, their microscale behaviour is scaled accordingly, thereby describing the overall functionality[6]. One common approach is to 'build' a picture of macroscopic foam drainage by 'adding' the hydrodynamic resistance of isolated channels and nodes in series[7]. It can be seen therefore, that any inaccuracies in the properties of these isolated systems propagate to a substantial degree of error when scaled to describe macroscopic systems.

Modelling foam channels using a theoretical framework represents the substantial majority of research undertaken in the area of foam channel drainage. However, even using simplified models to represent real systems has proved challenging, with results often conflicting[7,8]. This is largely due to the wide range of co-dependent variables involved in the process, which dramatically increases the complexity of the systems studied. For example, the surface rheology of foam channels is dependent on the shear imparted on it by flow of bulk liquid[9]; however, liquid flow rates vary with bulk liquid rheology and channel widths, which are themselves dependent upon the surface rheology and surface tension[10,11]. As such, one cannot treat any of these variables in isolation without directly measuring or resorting to assumptions regarding the others.

In addition to the difficulties faced by theoretical modelling, there are very few studies dedicated to the experimental measurement of microscale foam channels[12]. This means that any predictions that are made from microscale drainage models are difficult to assess for accuracy in real systems. This is largely due to the difficulties in effectively measuring such systems, which can be extremely difficult to isolate and effectively control in macroscopic foams[13].

More recently, studies of isolated PB and PB-Node geometries in bespoke experimental setups have provided an alternative to microscale measurements made from macroscopic foams. The superior control and repeatability provided by these systems has allowed for more detailed experimental studies into the co-dependence of PB bulk and surface parameters during microscale drainage. To date, isolated foam systems have been used to study a range of surfactants, including ionic and non-ionic low molecular weight (LMWS) systems[6,7,14-17], as

well as more limited investigations of protein and polysaccharide solutions[10]. While these studies have been able to identify fundamental differences in key parameters such as surface shear viscosity for different surfactant systems, the practical difficulties in measuring such systems still necessitate certain assumptions to be made.

A major assumption that features heavily in both microscale and macroscale foam drainage concerns the PB surface tension, which is an important parameter for determining bubble and channel dimensions, but is not measured *in-situ*. Instead, foam surface tensions are generally approximated based on the results of more conventional measurement techniques such as Wilhelmy Plate, Pendant Drop, Expanding Bubble, etc.[5]. It is generally considered, for example, that soluble LMWS solutions above their critical micelle concentration (CMC) produce foams with surface tensions approaching equilibrium, γ_e[18]. Recently however, measurements of isolated Tween 20 and Tween 80 PB geometries at constant liquid flow rates, have suggested this may not be the case, with the appearance of an apparent flow rate dependent surface tension[10].

The idea of time-dependent surface tension is certainly not new, and has been studied extensively for a wide range of surface-active species and concentrations[19-24], with solutions above the CMC being further influenced by the presence of micelles[25,26]. This dynamic surface tension (DST), γ, is primarily governed by the rate of adsorption of surface active molecules/particles to the air-liquid interface, where transport of surfactant molecules is either dominated by convection or diffusion. The dominant effect can generally be identified by solving the convective diffusion equation and using the Péclet's criterion to assess the relative magnitude of the terms[27,28]. In the case of soluble LMWS systems with static boundaries for example, adsorption is generally dominated by diffusion[20]. The rate of diffusion is highly dependent on the diffusivity of the LMWS species and the dimensions of the liquid channel, which therefore dictates how quickly surfactants are able to reduce surface tension when adsorbing at an interface.

The application of DST models to Plateau borders with liquid flow becomes far more complex, partially because of the geometry of the PB cross-section, but also because of the surface velocity of the PB interface. While a detailed physicochemical approach to the problem of PB drainage has been put forward by Durand*, et al.*[11], a means of experimentally validating these findings at the scale of individual Plateau borders remains elusive. In the more simplistic case of flow in horizontal liquid films, more experimental data is available, where the Marangoni effect describes the influence of surfactants on the hydrodynamics of the system, preventing localised thinning and therefore improving film stability[27-31]. More recently, the experimental examination of vertical films draining under the force of gravity have yielded interesting findings relating to the stability of thin films due to forced liquid flow[32] that may have parallels with forced flow in Plateau borders.

In the study of de Gennes[32], the impact of soap film drainage rates on surface tension and film stability is described. As the liquid flow increased, it was found that slower diffusing surfactants did not have time to adsorb at the air-water interface before exiting the film. These

films, with reduced surfactant concentration at the interfaces, were termed 'Young' films due to liquid flows being faster during the early stages of film drainage. It follows therefore, that such a mechanism is also likely to play a role in the stabilisation of PBs, where the inherently higher liquid flow rates would be expected to accentuate the effects seen by de Gennes[32]. If the majority of surfactant molecules were transported through the PB before being able to adsorb at the interface, then values of PB surface tension higher than γ_e could be expected, potentially lowering PB stability.

This study aims to provide a method that can assess the degree to which liquid flow rate could affect PB surface tension for high mobility surfactant species with well-characterised adsorption behaviour. The ability to control liquid flow rates through well-defined PB geometries using the experimental setup of Clarke*, et al.*[10] means that the 'ageing' of PBs should be effectively halted. As was shown for de Gennes[32] 'young' films, adjoining 'young' PBs could also suffer from reduced stability during the early stages of macroscopic foam drainage. As such, it is hoped that the current study will help to produce a more complete picture of the fundamental mechanisms underlying drainage and stability of LMWS macroscopic foams. Ultimately, this may prove valuable for researchers hoping to identify suitable surfactant species and concentrations for specific formulation applications.

Theory

Model Fitting to Geometric PB Profiles

In previous studies by Clarke*, et al.*[10],[14], the geometries of vertical, isolated PB's were measured at different forced liquid flow rates, Q, and fitted with solutions to the standard drainage theory[13,17] (Equation (1)). This dynamic equation accounts for the liquid flow through a PB tangential to the vertical axis, Z, with a radius, R, and the physical parameters I, D, ν, g, γ, and ρ denoting inertial and viscous flow parameters, kinematic viscosity, acceleration due to gravity, surface tension and bulk liquid density, respectively. The constant, c, is a geometric factor (~ 0.161) which can be used to describe the thin-film PB cross-section with area, $S = cR^2$ (See Figure 1c). The parameters D and I are dimensionless variables that describe the shape of the velocity flow field through the PB and ultimately depend on the surface rheology of the PB interface. Further information on these is given below and can also be found in the Supporting Information. The Supporting Information also gives a more complete description of Equation (1) and its derivation, in order to provide additional physical context.

$$\frac{dR}{dZ} = \frac{cD\nu Q - gc^2R^4}{\left(\frac{2IQ^2}{R}\right) - \left(\frac{c^2R^2\gamma}{\rho}\right)} \qquad \text{The standard drainage theory} \qquad (1)$$

As can be seen from Figures 1a) & 1b), measured PB profiles for LMWS systems have been shown to exhibit complex flow rate dependent geometries comprised of regions of relaxation and expansion. The geometric solution to Equation (1) for constant I and γ, as proposed by Clarke*, et al.*[10], was shown to account for both relaxation and expansion of the PB profile (see Figure 2) and is given by Equation (2). More information on the derivation and physical implications of Equation (2) can also be found in the Supporting Information of this study.

$$Z - Z_T = L\,ln\left[\frac{R^4\left({R_0}^4-{R_e}^4\right)}{{R_0}^4\left(R^4-{R_e}^4\right)}\right] + \frac{{L_c}^2}{4R_e}\left\{ln\left[\frac{R^4(R_0+R_e)^2\left({R_0}^2+{R_e}^2\right)}{{R_0}^4(R+R_e)^2\left(R^2+{R_e}^2\right)}\right] + 2\,tan^{-1}\left[\frac{R-R_0}{R_e\left(1+RR_0/{R_e}^2\right)}\right]\right\} \quad (2)$$

In this solution, the constant values of the inertial flow parameter, I, and surface tension, γ, result in values for an initial PB radius, R_0, according to Equation (3), that is located at a vertical offset, Z_T, from the top of the PB at $Z = 0$ (Figure 2). The PB equilibrium radius, R_e, is defined by Equation (4), describing the lower limit of the PB radius, at which gravity and viscous dissipation are balanced[17]. The vertical distance over which R_0 transitions to R_e is determined by the PB relaxation length, L, which is given by Equation (5). Finally, the variable L_c, refers to the capillary length defined as $L_c = \sqrt{\gamma/\rho\, g}$.

$$R_0 = \left(\frac{2\rho I Q^2}{c^2\gamma}\right)^{1/3} \quad (3)$$

$$R_e = \left(\frac{D\nu Q}{cg}\right)^{1/4} \quad (4)$$

$$L = \frac{IQ^2}{2c^2 g{R_e}^4} - \frac{\gamma}{4\rho g R_e} \quad (5)$$

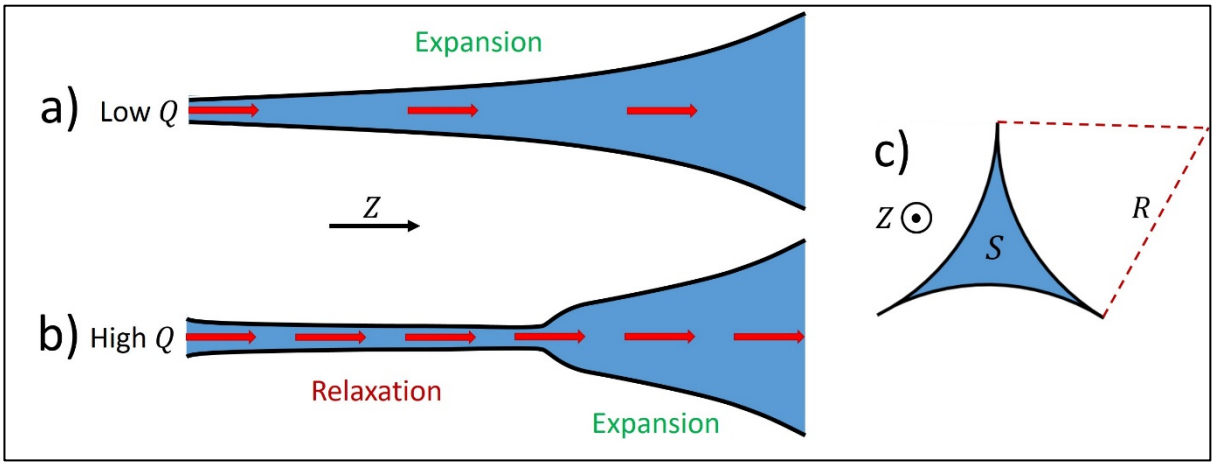

Figure 1. a) Typical low flow rate, Q, PB vertical cross-section for LMWS systems. **b)** Typical high flow rate PB vertical cross-section for LMWS systems. **c)** Thin-film PB horizontal cross-section with radius, R, and area, S.

Figure 2 shows that Equation (2) takes the form of a curve with two solutions for R for a given value of Z, and demonstrates the application to PB profiles exhibiting regions of relaxation and expansion similar to that in Figure 1b.

The study by Clarke, *et al.*[10] showed that a single set of physical variables for Equation (2) could be used to describe both expansion and relaxation regions of the PB, where it was assumed that the effect of variations in R would be small within a single PB. However, it was found that the agreement between theory and data decreased sharply for PBs at flow rates close

to the transition point between profiles of the type shown in Figure 1a to those in Figure 1b (i.e. relaxation only to combined relaxation AND expansion). Furthermore, analysis of the fitting parameters indicated the counterintuitive result that an *increase* in surface concentration of surfactant at the PB interface acted to *lower* its surface shear viscosity, μ_s. As such, it was deemed necessary to account for the impact of variations in R within a single PB in future studies.

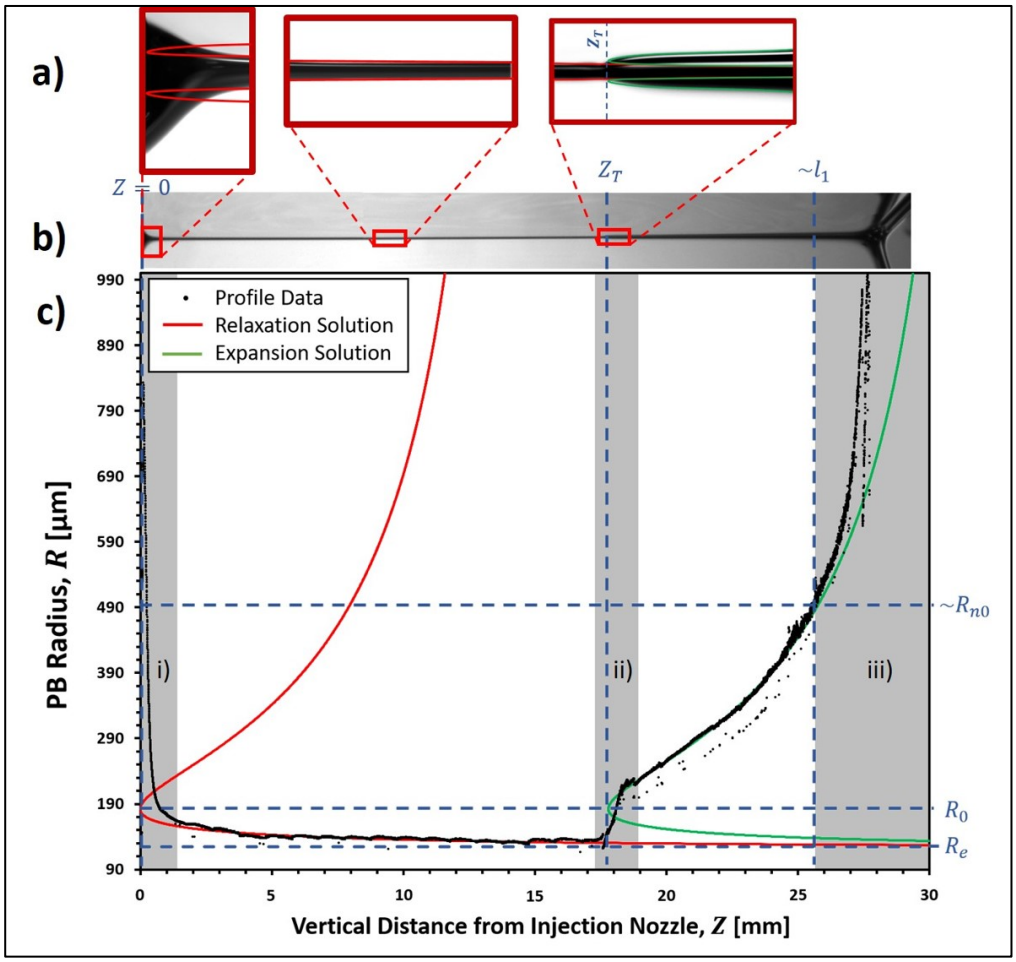

Figure 2. a) High magnification view of highlighted profile regions with visualisation of fitted curved overlaid. **b)** Low magnification PB profile image. **c)** Example of Equation (2) fit to profile data for a 182mM SDS solution at a flow rate of 100µl/min. Dashed blue lines indicate the position of key geometric variables. Grey shaded regions indicate poorly defined transitions/distortions, namely: **i)** the injection nozzle distortion around $Z = 0$, **ii)** the relaxation-expansion transition around Z_T, and **iii)** the PB to Node transition at l_1.

When one considers, the physical interpretation of the viscous and inertial flow parameters as describing the shape of flow velocity profiles through a horizontal PB cross-section, the need to account for R dependence in a single PB becomes clear. Equations (6) and (7) show the relationship between the velocity field of liquid flow through the PB[17], $\vec{u}(x, y)$, and the

viscous and inertial flow parameters obtained by averaging across the horizontal PB cross-section (see Elias*, et al.*[17] for details). At a constant liquid flow rate, the average flow velocity, $\bar{u}$, through an ideal horizontal PB cross-section can be calculated from Equation (8), such that the dependence of both D and I on PB radius is taken into account[17]. Note that in Equation (6), $\overline{\Delta u}$ describes the Laplacian of the velocity flow field averaged over the horizontal PB cross-section.

$$D = -R^2\overline{\Delta u}/\bar{u} \tag{6}$$

$$I = \overline{u^2}/_{\bar{u}^2} \tag{7}$$

$$\bar{u} = Q/cR^2 \tag{8}$$

In order to address R dependence during fitting, it was necessary to apply multiple fits of Equation (2) to PBs with regions varying significantly in average PB radius. This is a consequence of the discrete nature of Equation (2), which assumes constant values for all of the variables contained within the fitting region. In reality, a perfect fit to any real PB system would require the division of the PB into an infinite number of sections with an infinite number of solutions, however; this would obviously be impractical for experimental purposes. Instead, the criteria of an R-Squared value greater than 0.9 was used to designate a 'good' fit of a solution to a region of the PB geometry. This criterion meant that a maximum of four solutions to Equation (2) could provide a 'good' fit to the full length of any observed PB geometry. Note that these solutions neglected the distortion regions (i) and (ii) shown in Figure 2.

The approximation of constant variables within each discrete fitting region of the PB has some important physical implications, particularly with regard to the assumption of constant surface tension. Using this method, it is possible to determine magnitudes and changes in surface tension over the length of the vertical PB based discrete changes in γ for each fitting region. However, as the overall gradient in surface tension, $\nabla\gamma$, is neglected, this model also neglects contributions due to Marangoni stresses that would arise from these gradients. While the variations in γ are expected to be small for the systems that will be studied here, this is an important point for future studies, wherein a dynamic version of Equation (2) will be required in order to account for these effects.

Dynamic Surface Tension as a Model Parameter

In order to identify the potential impact of liquid flow rates, Q, on the DST in these isolated PB systems, it is necessary to determine whether surfactant transport to the interface is dominated by convection or diffusion. Only then can an appropriate model describing surfactant adsorption rates be selected.

In the case of immobile PB interfaces, the geometry of the channel cross-section is such that the Péclet number would be expected to vary between diffusion dominated and convection dominated surfactant transport depending on position (i.e. Péclet numbers varying between

$P_e \ll 1$ and $P_e \gg 1$ respectively)[33]. This can be simply approximated based on the standard equation $P_e = U_0 H/D_s$ where U_0 describes the fluid velocity relative to the immobile interface, H describes the channel width, and D_s is the diffusion coefficient of the surfactant[33]. The channel width inside an ideal Plateau border with thin films varies between $0 < H \leq (\sqrt{3}-1)R$ giving a maximum range of $0 < P_e < u(\sqrt{3}-1)R/D_s$. Approximating u based on the cross-sectional average shown in Equation (8), and with maximum flow rates $Q = (\vartheta)10^{-12}$, minimum radii, $R = (\vartheta)10^{-5}$, and minimum surfactant diffusivity, $D_s = (\vartheta)10^{-12}$, yields a maximum range of $0 < P_e < (\vartheta)10^{5}$.

Despite the significant potential variation between convective and diffusive surfactant transport shown, the case of an immobile interface is far from that expected for highly mobile, soluble LMWS species such as Tweens and Sodium dodecylsulfate (SDS) [10,14,20,34]. In these cases, the dominant flow profile is expected to be plug-flow, where $U_0 \rightarrow 0$ (i.e. a stationary mode) as perfect plug-flow is approached. In this limiting case therefore, diffusion would be expected to be the dominant mode of surfactant transport. Indeed, in the majority of literature describing adsorption of LMWS systems, diffusion is found to be the dominant mode[20], with diffusion coefficients measured based on this finding[22].

While a far more in depth treatment of this problem is possible by solving the convective diffusion equation for the PB system, the treatment above was deemed sufficient for the purpose of this study using highly mobile LMWS systems exhibiting Plug-like flow[10,14]. As such, the Ward-Tordai (W-T) model for diffusion-controlled adsorption was adopted, which has been previously applied to successfully describe the kinetics of ionic surfactants with high surface concentrations[19].

The expressions describing the W-T model used here are given by Equations (9) and (10), expressing the short-time and the long-time approximation regions with ideal ionic activity (IIA) correction, respectively[19,35].

$$\gamma_{ST}(t) = \gamma_0 - 2C_0 R_g T\sqrt{D_s t/\pi} \qquad \text{Short Time Approximation} \qquad (9)$$

$$\gamma_{LT}(t) = \gamma_e + nR_g T\left(\frac{\Gamma_e{}^2}{C_0}\right)\sqrt{\frac{\pi}{4D_s t}} \qquad \text{Long Time Approximation with IIA Correction} \qquad (10)$$

The surface tensions, γ_0 and γ_e, describe the pure solvent surface tension (in this case water) and the equilibrium surface tension of the surfactant solution with concentration, C_0, respectively. The molar gas constant is denoted by R_g, while the temperature is given by T. The equilibrium surface excess, Γ_e, describes the equilibrium concentration of surfactant at the air-water interface, and can be influenced by the electrostatic interactions of charged species. The correction factor, n, was introduced to the W-T long time approximation by Kinoshita*, et al.*[19] in order to account for the action of ionic surfactants. For non-ionic surfactants (e.g. Polysorbates) $n = 1$, whereas for a univalent ionic surfactant in the absence of supporting electrolyte (e.g. SDS in aqueous solution) $n = 2$. No IIA corrected form of the W-T short time approximation is currently available in the literature; however, such a derivation would only

be required for the analysis of charged species in their short time region. As the only charged species analysed in this study was SDS, it will be shown that its very small short time approximation region ($t \ll 10$ms)[19] meant that only the IIA corrected long time approximation was required in this case.

Having identified a suitable models of surfactant diffusion, it was necessary to identify a means of measuring values for t that could be used in conjunction with the fitting of Equation (2) to measured PB profiles. Given that the fitting of Equation (2) required PB profiles to be broken down into discrete regions with constant surface tension, it was therefore necessary to measure an average value for t over each discrete profile section.

When surfactant solution is injected at constant Q directly into the PB at $Z = 0$, the resulting average velocity in a given PB section is dependent upon that region's average radius, i.e. $V = \bar{u}(R = \bar{R})$. Therefore, for a surfactant molecule travelling with the bulk liquid, its average residence time in that PB region, τ_{Res}, can be approximated by the distance over velocity relationship shown in Equation (11).

$$\tau_{Res} \approx {}^{c\bar{R}^2 Z}/_{Q} \tag{11}$$

While Equation (11) is a suitable approximation for a PB with an ideal cross-section (see Figure 1c), this is not the case for the systems studied here. Instead, the PB cross-section becomes ill-defined as it approaches the liquid injection nozzle at $Z = 0$, transitioning from an ideal geometry to an approximately cylindrical one[14,17] over a distance, Z_D (See Figure S1).

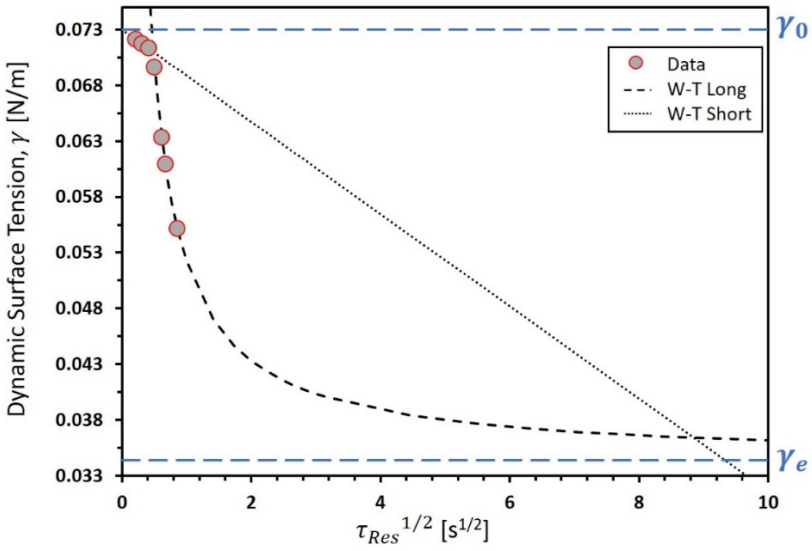

Figure 3. Example of short time and long-time with IIA W-T approximations of DST for an uncharged surfactant species (Tween 20). Example data points were taken based on $\gamma(\tau_{Res}) = \min\left[\gamma_{ST}(\tau_{Res}), \gamma_{LT}(\tau_{Res})\right]$. Maximum and minimum values of surface tension are given by the surface tension of water, γ_0, and the equilibrium surface tension, γ_e, respectively.

In order to account for this effect, Equation (11) was amended to Equation (12), giving equal weight to the ideal and cylindrical geometries in the distortion region. PB radii in the distortion region were given the notation R_D.

$$\tau_{Res} \approx \frac{c\bar{R}^2}{Q}(Z - Z_D) + \left(\frac{\overline{R_D}^2(16c+3\pi)}{32Q}\right)Z_D \tag{12}$$

Using the approximation that $t = \tau_{Res}$, values for $\gamma_{ST}(\tau_{Res})$ and $\gamma_{LT}(\tau_{Res})$ can be calculated using literature values of D_s and Γ_e from Equations (9) and (10). The best approximation for $\gamma(\tau_{Res})$ was then based on the minimum of the two values, such that $\gamma(\tau_{Res}) = \min[\gamma_{ST}(\tau_{Res}), \gamma_{LT}(\tau_{Res})]$. As can be seen in the example for an aqueous solution of Tween 20 in Figure 3, this produced a natural transition between short and long time approximations at the crossover of Equations (9) and (10). At times below the crossover, DST was described by γ_{ST}, while above the crossover DST was described by γ_{LT}.

PB Surface Viscosity

The previous studies by Clarke, *et al.*[10],[14] have consistently indicated that PB surface viscosity for LMWS systems exhibits a significant degree of surface shear thinning. Indeed, such a result has also been suggested by Gauchet, *et al.*[18] to account for their findings in addition to potentially be responsible for the large variation in literature values for SDS surface viscosity. This was proposed by Clarke, *et al.*[10] to be a consequence of variations in the PB surface tension, however; results counterintuitively indicated that surface shear viscosity *decreased* with *increasing* interfacial surfactant concentration[10]. In order to address whether the theory proposed here was able to account for this behaviour, it was necessary to calculate the surface viscosity, μ_s, and average liquid shear rate, $\bar{\dot{\gamma}}_s$.

PB surface viscosity can be calculated for an equilibrium PB by combining Equations (4), (13) and (14)[10,14].

$$D^{-1} = c\left[0.02 + \frac{0.0655{B_0}^{-0.5}}{0.209+{B_0}^{0.628}}\right] \tag{13}$$

$$\mu_s = B_0\mu R \qquad \text{(with } R = R_e\text{)} \tag{14}$$

Equation (13) is the phenomenological expression proposed by Nguyen[36] to calculate the dimensionless Boussinesq Number, B_0, from the viscous flow parameter, D. Subsequently, B_0 can be converted into its dimensional counterpart, the surface viscosity, using the dynamic bulk viscosity, μ, via Equation (14). In previous studies, Equation (14) is presented in an alternative form, $M = \mu R/\mu_s$, where the dimensionless parameter, M, was one of four dimensionless groups first derived by Leonard, *et al.*[37] as a solution to the velocity profile through a Plateau border. This parameter was later described as the relative surface mobility by Kraynik[38] who noted that: 'the use of surface viscosity to describe interfacial mobility should not be viewed as exact because the Boussinesq surface fluid is a relatively simple model of the interfacial

region'. Subsequently, B_0 has been used to describe the inverse of the relative surface mobility[17,36] thereby yielding the form of Equation (14) presented here.

In order to better understand the relationship between PB surface tension and μ_s, the dependence of surface tension on PB radius first had to be taken into account. As Equations (13) and (14) are only valid under equilibrium PB conditions (i.e. $\mu_s(R = R_e)$), it follows that a direct link to surface tension can only be made for the case $\gamma(R = R_e)$. However, as the 'infinite' PB geometry, $R = R_e$, is a theoretical ideal case, only approximations of the relationship between surface tension and surface viscosity could be made here. Therefore, only fitted surface tensions extracted from PB regions where the minimum radius, R_{min}, approached the corresponding fitted R_e (i.e. $\gamma(R_{min} \to R_e)$), were deemed suitable for analysis in this instance.

Calculation of the average shear rates through equilibrium PB were undertaken using the approximation[17] shown below:

$$\bar{\dot{\gamma}_s} \approx \frac{Q}{cR_e{}^3} \tag{15}$$

Experimental

Preparation of Surfactant Solutions

SDS (>99.9%) from Fisher Scientific (Loughborough, UK), Tween® 20 and Tween® 80 from Sigma-Aldrich (UK), were weighed and magnetically stirred at room temperature with 15.0MΩ·cm purified water. Stirring continued for a minimum of 30 minutes prior to use of the solution to ensure the complete dissolution of surfactant.

These surfactants represent both charged (SDS) and non-ionic (T20/T80) species that are commercially significant and have therefore been well studied in literature[19,20,22,34,39-42]. Despite some variation in reported values of D_s and Γ_e due to variations in the composition of Tween systems and the presence of impurities in SDS, these surfactants were still deemed the most suitable for the present study. This was partially due to the bulk of available literature examining their adsorption dynamics, but also in order to directly compare the findings of the revised analysis presented here with those in previous studies using this experimental setup[10,14]. Furthermore, the substantial difference in critical micelle concentration (CMC)[42,43] and rates of adsorption[19,22] between the Tweens and SDS were expected to yield observable differences in PB behaviour. It should be noted however, that in order to improve the precision of the current technique in future studies it will be necessary to select surfactants with highly consistent purity and composition.

Characterisation of Surfactant Solutions

Each surfactant solution was studied at two different concentrations (see Table 1). Concentrations of SDS were chosen to represent ~2× and ~20× the CMC according to

literature values[22,42-44], however it was necessary to amend this to ~10× and ~20× the CMCs of T20 and T80 due to the poor PB stability in the experimental setup at lower concentrations.

Values for D_s and Γ_e of each surfactant were taken from representative values produced by dedicated experimental studies of DST in literature[19,22]. These values can also be found in Table 1, where it can be seen that the diffusion coefficients for SDS were approximately 100× larger than those for the Tween systems, suggesting much faster rates of SDS adsorption than Tween adsorption. It should be noted here that the decreasing values of D_s with increasing surfactant concentration made by Bąk, *et al.*[22] for the Tweens is in agreement with observations made by other authors for different non-ionic surfactants[45-48]. This decrease is most likely due to the increasing number of micelles formed with increasing surfactant concentration above the CMC[49], where monomer exchange with micelles increasingly dominates over monomer diffusion to the interface[50].

Surfactant	C_0 [mM]	Γ_e [mol/m^2]	n	D_s [m^{2}s^{-1}]
Tween® 20[22]	0.61	3.50×10^{-6}	1	7.00×10^{-12}
	1.22	3.50×10^{-6}	1	1.50×10^{-12}
Tween® 80[22]	0.15	2.20×10^{-6}	1	10.00×10^{-12}
	0.30	2.20×10^{-6}	1	2.00×10^{-12}
SDS[19]	17.40	6.75×10^{-6}	2	5.30×10^{-10}
	182.00	6.75×10^{-6}	2	5.30×10^{-10}

Table 1. Characterisation of surfactant property variables for aqueous solutions of T20, T80 and SDS based on representative literature values[19,22].

A Krüss Processor® Tensiometer K100 (Krüss GmbH, Germany) with density hook attachment and silicon density standard was used to measure liquid density, while surface tension was measured using a Wilhelmy Plate attachment. The solution dynamic viscosity was measured using a Malvern Kinexus® Pro rheometer (Malvern Panalytical, UK) with Double-Gap geometry, which provided excellent measurement sensitivity for the low viscosity solutions studied here. All measurements were carried out at $T = 295$K, and presented data are average values with absolute errors of one standard deviation.

The PB-Node Setup

In order to create the isolated PB's required for analysis at controlled liquid flow rates, the isolated PB-Node setup of Clarke, *et al.*[14] was used. More details of this setup can be found in literature[10,14], however it relies on the principle of a closed tripod frame that can be withdrawn from surfactant solution to produce and arrangement of liquid films that terminate

in a spatially 'ideal' PB and node (see Figure 4). PBs were directly injected with additional surfactant solution at controlled liquid flow rates (20µl/min $\leq Q \leq$ 180µl/min) and imaged, to create geometric PB profiles of PB radius, R, vs. height below the liquid injection nozzle, $0 \leq Z \leq l_1$ (see Figure 2).

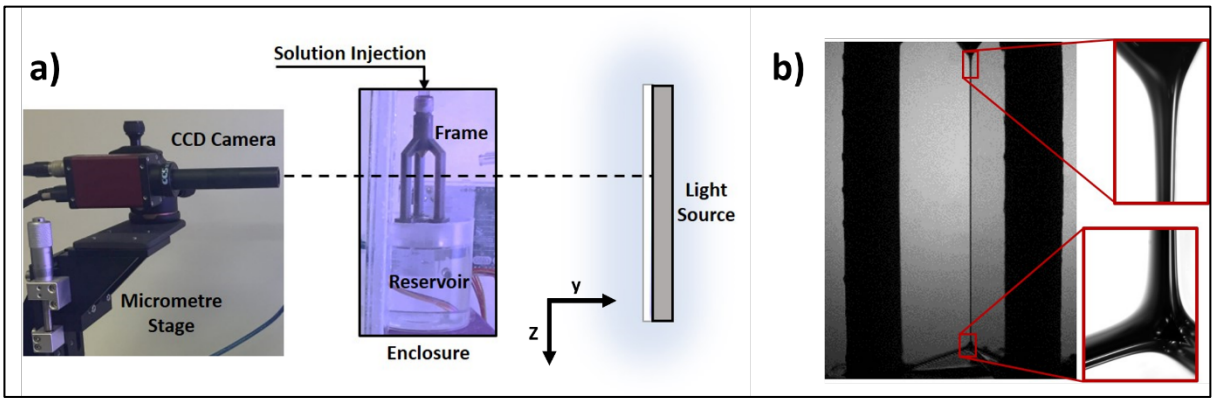

Figure 4. The isolated PB-Node setup of Clarke*, et al.*[14]. **a)** Imaging setup showing camera, frame setup and rear light source. **b)** Images of PB/node profiles at different magnifications, with the highest resolution of 1.5µm per image pixel. Reprinted with permission from C. Clarke, A Lazidis, F Spyropoulos, and I. T. Norton, "Measuring the impact of channel length on liquid flow through an ideal plateau border and node system," Soft Matter 15, 1879–1889 (2019). Copyright 2019 The Royal Society of Chemistry.

Model Fitting

Due to difficulties in utilising automated fitting methods, as discussed in previous work[10], manual fitting of Equation (2) to PB profile sections was able to consistently produce good agreement between theory and experimental data.

Measured PB profiles were divided into a maximum of four fitting regions, based on a coverage of the PB profile from $0 \leq Z \leq l_1$ with a minimum R^2 value of 0.9 being required for each solution. These solutions did not include the distortion regions (i) and (ii) in Figure 2 as discussed above. Examples of dividing PB profiles into fitting regions in order to calculate their respective surfactant residence times, τ_{Res}, can be found in Figure S2.

Results

Solution Properties

The measured surfactant solution parameters as well as those taken from representative literature are presented in Table 2. As anticipated, the dynamic viscosity of solutions was only slightly higher than that of pure water at $\sim 8.9\times10^{-4}$ Pa·s at 25°C[51]. Values for the equilibrium surface tension were in good agreement with those found in existing literature[19,22,44,52-55]. This provided increased confidence that the literature values[19,22] for Γ_e and D_s in Table 1 were reasonable representations of the surfactant behaviour in this study. A trend of decreasing surface tension with increasing surfactant concentration above the CMC was observed for all surfactants, however this variation was within the measurement errors shown for the tween systems and is often seen in literature for SDS systems[19,44,55]. This may represent the effect of trace impurities (e.g. lauryl alcohol), which are common in SDS systems. However, as the measured SDS surface tensions were almost identical to those measured by Kinoshita*, et al.*[19] from which Γ_e and D_s were taken, these were still determined to be a good representation of the system in this study.

	Surfactant Concentration [mM]	**Density [mg/ml]**	**Viscosity [Pa·s] (10^{-4})**	**Equilibrium Surface Tension [mN/m]**
Tween® 20	0.61	997.70 ± 0.30	9.56 ± 0.07	36.3 ± 0.2
Tween® 20	1.22	997.90 ± 0.10	10.23 ± 0.48	35.9 ± 0.5
Tween® 80	0.15	997.90 ± 0.10	8.84 ± 0.03	40.0 ± 0.5
Tween® 80	0.30	997.60 ± 0.40	9.69 ± 0.23	39.2 ± 0.5
SDS	17.40	998.70 ± 0.90	9.84 ± 0.05	37.9 ± 0.1
SDS	182.00	1005.00 ± 0.50	13.65 ± 0.14	35.4 ± 0.1

Table 2. Averaged measurements of surfactant solution bulk and surface properties.

Relaxation-Expansion Model

Fitting of Equation 2 to PB profiles was carried out in accordance to the theory and procedure outlined above. A maximum of four fits was applied to any one PB profile, providing an excellent description of its geometry. Average R^2 values were consistently in excess of 0.9 for all liquid flow rates. This marked a significant improvement on previous fit quality[10], where flow profiles transitioning between types in Figure 1a and 1b were poorly characterised. Figure 5 shows the fits applied to profiles of 17.4mM SDS, 0.61mM T20 and 0.15mM T80 at $Q =$ 20µl/min and $Q =$ 100µl/min, with corresponding values for the inertial flow parameter, I, shown.

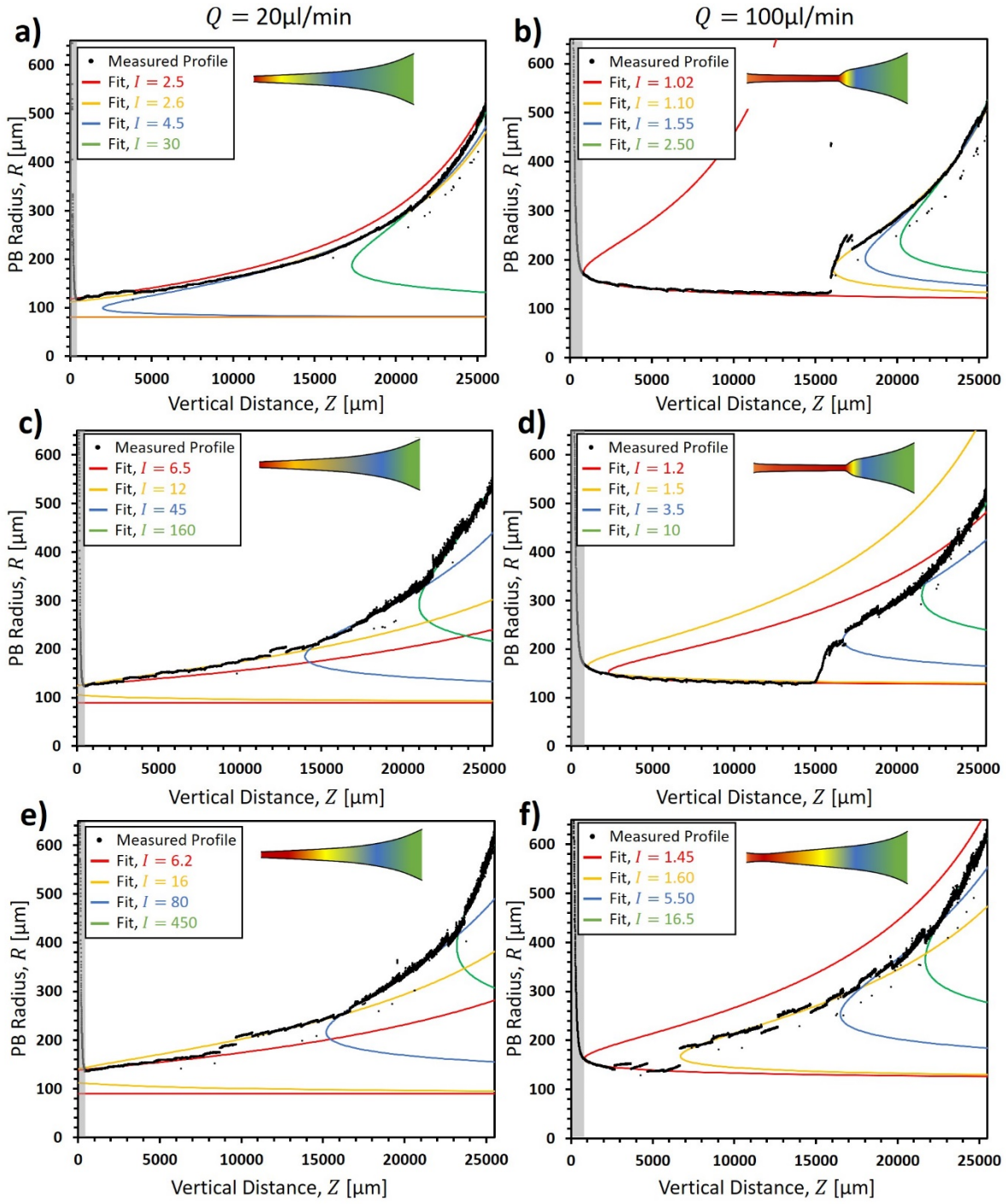

Figure 5. Fits of Equation (2) to PB profiles for: **a)**, **b)** 17.4mM SDS; **c)**, **d)** 0.61mM T20; and **e)**, **f) 0**.15mM T80. **a)**, **c)** and **e)** are for liquid flow rates of Q = 20µl/min. **b)**, **d)** and **f)** are for liquid flow rates of Q = 100µl/min. Inset diagrams provide visualisations of the behaviour of I along the equivalent vertical PB cross-sections.

Inertial Flow Parameter

Values for the inertial flow parameter, I, were shown to exhibit a strong linear relationship with $1/V^2$, taking the form $I = (m/V^2) + 1$ with m being the gradient of the straight line (see Figure 6). This appeared to reflect the $1/u^2$ dependence of I in Equation (7). The intercept of 1 is a key physical limit of, I, where the relationship measured here of $I \to 1$ as $D \to 0$ represents the tendency of these systems towards ideal plug-flow through the PB. This was in line with the expected behaviour of high mobility surfactants.[34,56] Little discernible difference was observed in these relationships due to bulk surfactant concentration; however, a clear difference in gradient was seen between the Tween and SDS systems. The average gradient of SDS solutions compared to that of Tween solutions was $m = 0.003$ and $m = 0.037$ respectively, suggesting flow profiles of Tween systems to be more Poiseuille-like than SDS.

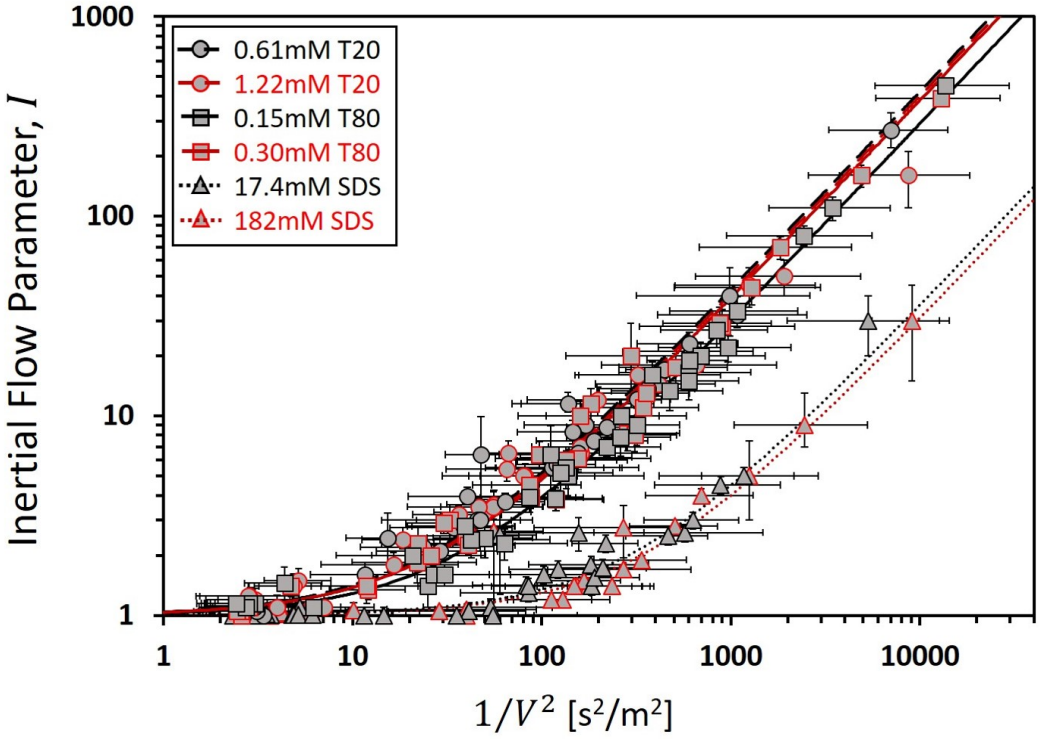

Figure 6. Values of the inertial flow parameter, I, as a function of the inverse square of the average flow velocity in the fitting region, $1/V^2$. Linear fits to data take the form of $I = (m/V^2) + 1$ where m is the gradient of the straight line.

Dynamic PB Surface Tension

PB residence times were calculated as outlined above, and then used to calculate PB DST using Equations (9) and (10), with $t = \tau_{Res}$. As SDS has been extensively studied using other experimental techniques, it was possible to directly compare the DST values calculated here with those measured in literature[19,20]. DST calculated for 17.4mM SDS was the most

comparable, with measured literature DST available for 15mM and 10mM samples. This showed a very strong agreement (see Figure S3) and confirmed that only the IIA corrected form of the W-T long time approximation (i.e. Equation (10)) was required for this study.

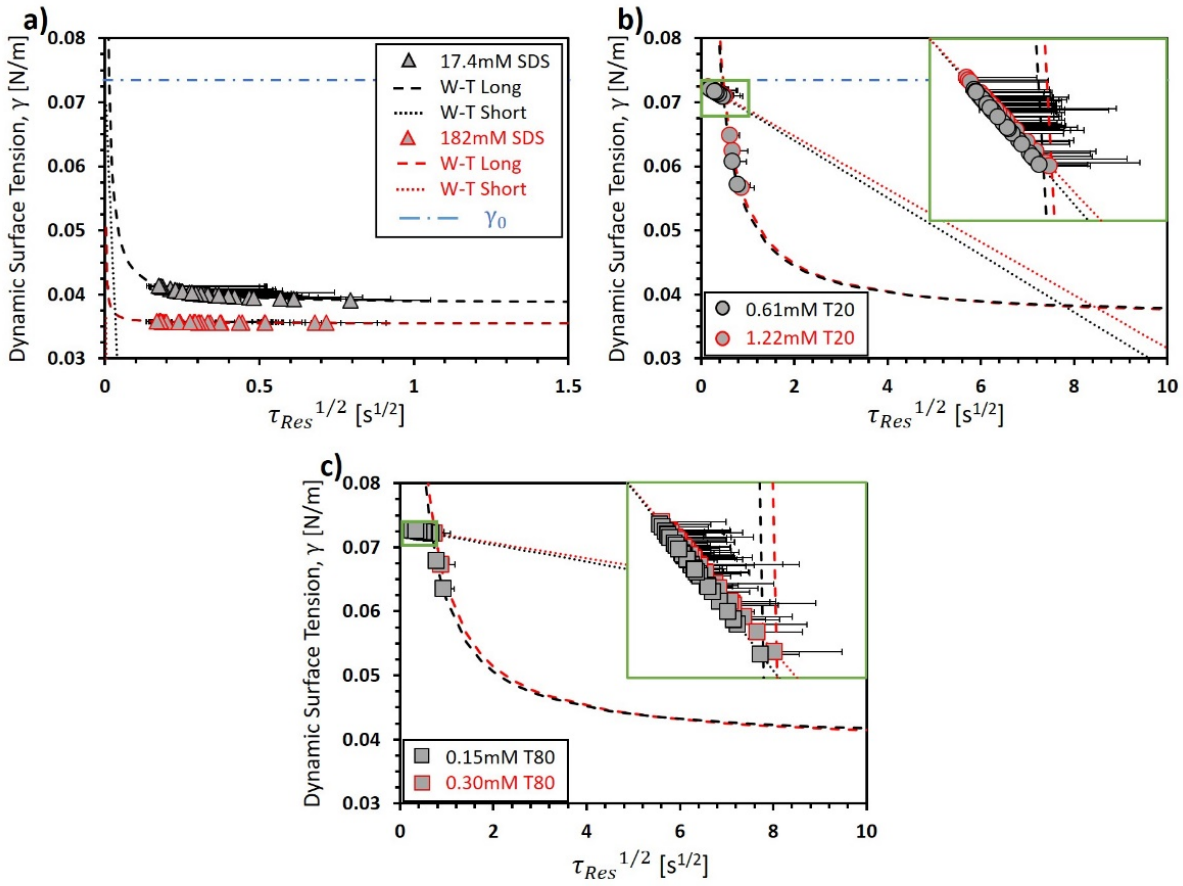

Figure 7. Calculated DST, γ, of **a)** SDS, **b)** T20 and **c)** T80 based on the average PB residence time of surfactant molecules, τ_{Res}. Errors are not shown for γ, as data points would follow the lines of the W-T long and short time approximations shown for any changes in $\tau_{Res}{}^{1/2}$.

Figure 7 highlights the dramatic differences between γ for SDS and Tween solutions, which result from the faster adsorption rates of SDS. While SDS approached γ_e within its PB residence times ($\gamma \to \gamma_e$), the Tween systems at many Q's remained closer to the surface tension of pure water ($\gamma \to \gamma_0$). This implied that for high fluid velocities, the rate of adsorption of T20 and T80 resulted in poor surfactant coverage of the PB interface. Indeed, this would explain why lower concentrations of Tweens than those used here were unable to produce stable PBs for analysis, and why even at higher concentrations, PBs of both T20 and T80 were more prone to collapse than those of SDS.

When discussing PB stability, it must be remembered that the collapse of these systems is primarily attributed to the rupture of films adjoining the PB rather than the breaking of the PB itself. As the liquid flow rates through adjoining films are generally considered significantly

smaller than those through PBs[57], it could be expected that surfactant residence time in these films was higher and thereby resulted in lower film surface tension. In this instance, one would expect the presence of Gibbs Marangoni forces due to the resulting concentration gradient of surfactant between film and PB interfaces[58]. The questions concerning stability therefore, relate to the extent of this concentration gradient and the rate at which surfactants could diffuse from the adjoining film interfaces to those of the PB. When one considers that film drainage has also been shown to result in 'younger' interfaces, the suggestion is that in the very early stages of foam drainage, slower adsorbing LMWS may provide little contribution to foam stability. Answering such questions is beyond the scope of the current study, however could be highly relevant in assessing foamability and short timescale stability of LMWS foams.

It has already been noted that the assumption of homogeneous surface tension in each of the separate PB fitting regions prevents an analysis that includes Gibbs-Marangoni Effects in this instance. However, it is clear from Figure 7 that the variation in surfactant residence times calculated here would result in vertical surface tension gradients, $\nabla\gamma$, along the PB. Indeed, this was seen from the differences in surface tension between neighbouring sections of PB. As the surface coverage of the PB increases with increasing Z (i.e. increasing t), the resulting Marangoni stresses would be expected to oppose the concentration gradient, therefore opposing liquid flow. In this respect therefore, it would be expected that the role of Marangoni forces would decrease bulk flow velocities adjacent to the interface, thereby increasing surfactant residence times and reducing the surface tension gradient. While the results presented here therefore provide a good indication of the expected magnitudes of PB surface tension, a full dynamic equation describing the PB profile geometry is still required in order to enact precision measurements of the physical parameters described here.

A more general issue regarding the calculation of PB surface tensions for PB profiles was the errors involved in calculating timescales, t. As can be seen from Figure 7a, the errors in τ_{Res} for SDS would have had little impact on the calculated γ according to the W-T approximations. However, Figure 7b shows that the errors in τ_{Res} for T20 and T80 could have resulted in decreases in γ of up to 15%, making this a significant source of error for these systems. As the bulk of the error in τ_{Res} originated from the approximation of the PB geometry between $Z = 0$ and $Z = Z_D$ (see Figure S1), this highlights the need for the precise characterisation of the full PB geometry, regardless of the subsequent method of analysis.

PB Surface Viscosity

When comparing γ with PB surface shear viscosity, μ_s, Clarke*, et al.*[10] found the counterintuitive result that μ_s *decreased* with *increasing* surfactant concentration at the interface. Figure 8 shows that this was no longer the case when the theory proposed here is applied. The plotted data points represent values extracted from PB fitting regions where the minimum radius was approaching the equilibrium radius (i.e. $R_{min} \rightarrow R_e$). As discussed previously, the closer the values of R_{min} to R_e, the more reliable the visual relationship between γ and μ_s. As such, data points are categorised in to those whose R_{min} were ≤10% (green),

≤15% (orange) and ≤20% (red) greater than their R_e values, therefore helping to provide an indication of the strength of the trends.

The extrapolation of data trends in Figure 8 are clearly largely approximated, however; the purpose here was to show that relationships similar to those observed between surface tension and other surfactant concentration variables (e.g. bulk concentration, surface concentration[19,22]) fit well with the data here. Ultimately, this suggests the far more intuitive result that surface viscosity *increases* with *increasing* surfactant concentration at the PB interface. This relationship exists between the two extremes of a clean air-water interface with a surface viscosity of zero, and a surfactant saturated air-water interface with a corresponding maximum surface viscosity depending on the surfactant species. While maximum μ_s for T20 and T80 could not be established based on the data here, the maximum μ_s for SDS was suggested to be $\sim 1 \times 10^{-8}$g/s. This is in line with the previous lower limit set by Clarke, *et al.*[14], as well as the high precision measurements made by Zell, *et al.*[34], whose studies of planar interfaces showed that soluble LMWS systems (including T20 and SDS) had surface viscosities lower than the measurement sensitivity of existing techniques (i.e. $\mu_s < 10^{-5}$g/s).

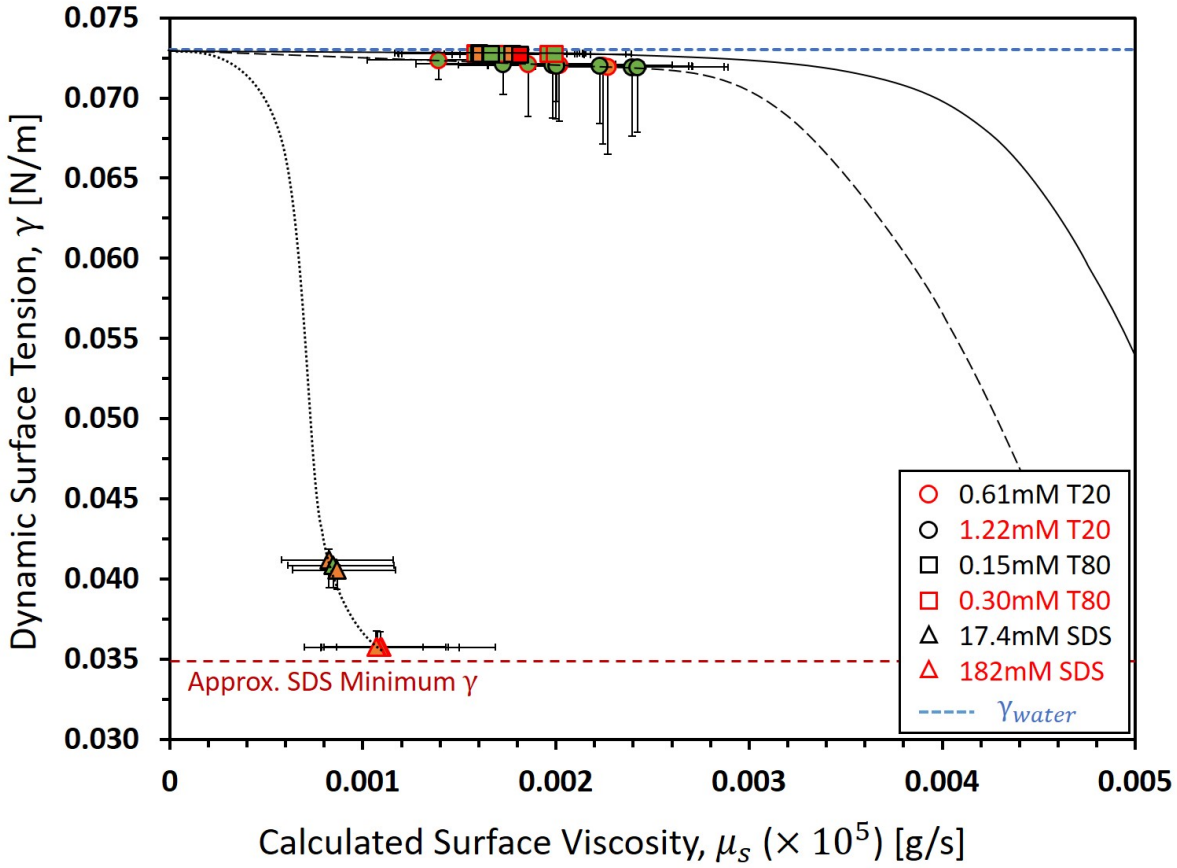

Figure 8. Calculated DST, γ, vs. calculated surface viscosity, μ_s, for concentrations of SDS, T20 and T80. Fill colours of data points represent how close values of R_{min} were to R_e with R_{min} ≤+10% (green), ≤ +15% (orange) and ≤ +20% (red). Black lines indicate suggested trends based on standard surface tension vs. surfactant concentration relationships.

It is also clear from the revised theory applied here, that the apparent surface shear thinning observed by Clarke, *et al.*[10],[14] for both SDS and Tween systems was likely to have been largely a result of the restrictions imposed on fitting variables in these cases. Data from this study showed that μ_s was virtually independent of average liquid shear rate at the concentrations and liquid flow rates studied, with any variations in μ_s that did occur being attributed to changes in surface tension (see Figure 9).

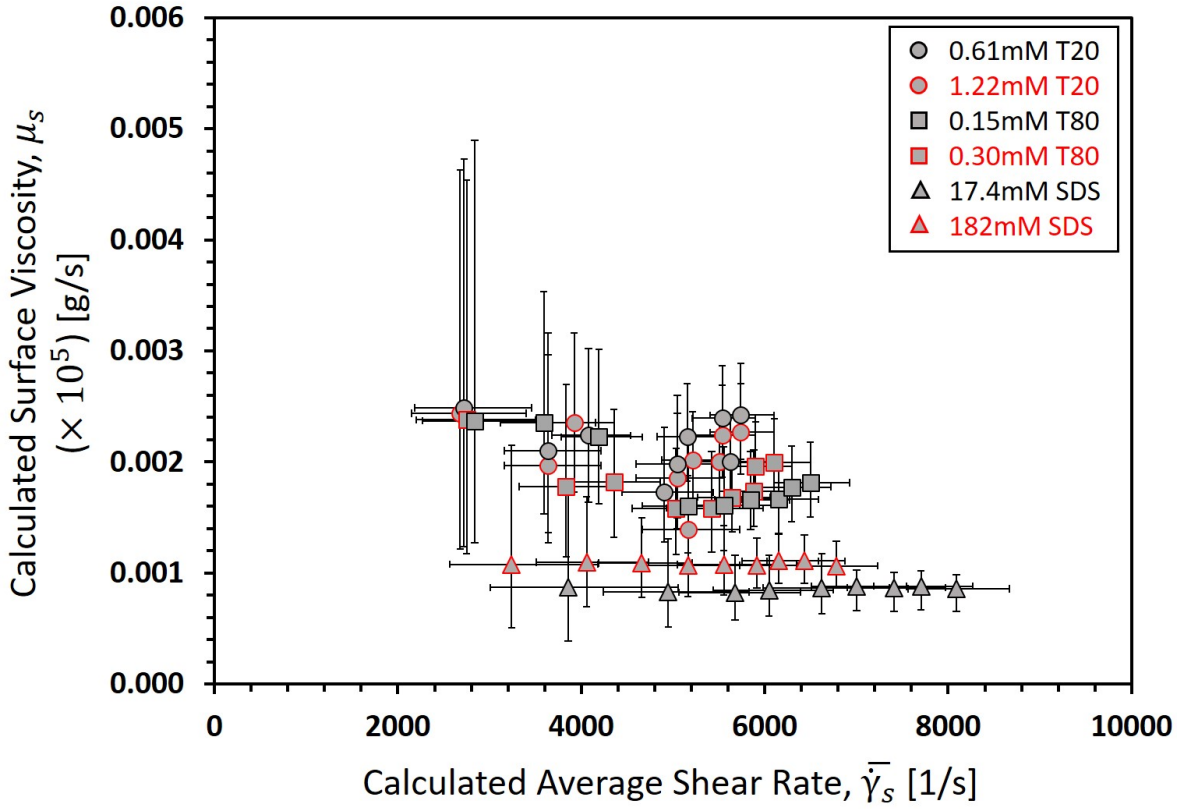

Figure 9. Calculated surface viscosity, μ_s, vs. calculated average liquid shear rate, $\bar{\dot{\gamma}}_s$ for SDS, T20 and T80 solutions.

Conclusions

The novel experimental setup of Clarke, *et al.*[10],[14] was further investigated for the soluble surfactants SDS, T20 and T80. The hypothesis that increasing liquid flow velocity through ideal isolated Plateau borders of a foam microstructure could result in 'younger' PB interfaces was assessed using a novel analytical technique. Analysis of measured PB profiles indicated that the average timescales over which soluble LMWS molecules could reside in the PB were similar to those required for surfactant molecules to diffuse to the air-water interface. As such, the adsorption kinetics of each surfactant were shown to play a major role in the flow rate dependence of PB geometries and their stability.

The liquid flow rates resulting in the highest DST were always in the range 40µl/min$< Q <$100 µl/min, which is within the range of liquid flow rates generally observed during macroscopic foam drainage. This implies that LMWS surfactants with longer adsorption timescales could have detrimental effects on macroscopic foam stability during the early stages of foam drainage. This effect is likely to be compounded by the adjoining 'young' films also formed at this stage[32].

The physical parameters derived from the present model each PB system were consistent with those expected for high mobility LMWS. Liquid flow profiles tended towards plug-flow, with surface shear viscosity for all systems at levels far below the measurement sensitivity of existing direct measurement methods, as proposed by Zell*, et al.*[34]. The increase in surface viscosity increased with surface surfactant concentration, while showing no discernible relationship to liquid shear rate. As such, the refinement of the model and fitting procedure in this study was able to address the counterintuitive findings of previous work[10,14].

The present study demonstrates how the geometric analysis of controlled, isolated, foam systems has the potential to yield precision data regarding their complex and dynamic nature. A static geometric profile solution is able to provide a good description of vertical PB profiles at constant liquid flow rates, however a complete approach requires that the dynamic nature of the interface be taken to account in a dynamic geometric profile equation. Only then can the full potential of this technique be realised.

Supporting Information

The following files are available free of charge.

Figure S1. Characterisation of PB distortion between $Z = 0$ and $Z = Z_D$, where PB geometry transitions from an approximately circular to an ideal PB cross-section. Left – Image of PB distortion. Right – Schematics of the corresponding 2D and 3D cross-section geometries. (TIFF)

Figure S2. Example of PB profile divided into PBs fitting regions to calculate their respective surfactant residence times, τ_{Res}. (TIFF)

Figure S3. Comparison of calculated DST, γ, of 17.4mM SDS using the W-T long time approximation with IIA correction with $t = \tau_{Res}$, in comparison to experimental values for 10mM SDS[19] and 15mM SDS[20] from existing literature. (TIFF)

Abbreviations

CCD, Charged Coupled Device; CMC, Critical Micelle Concentration; DST, Dynamic Surface Tension; IIA, Ideal Ionic Activity; LMWS, Low Molecular Weight Surfactant; PB, Plateau border; SDS, Sodium dodecylsulfate; T20, Tween 20; T80, Tween 80; W-T, Ward-Tordai.

References

1 J. Wang; A. V. Nguyen; S. Farrokhpay, A Critical Review of the Growth, Drainage and Collapse of Foams, *Advances in Colloid and Interface Science* **2016**, *228*, 55-70.

2 R. J. Pugh, *Bubble and Foam Chemistry*; Cambridge University Press: Cambridge, United Kingdom, **2016**.

3 E. Dickinson, 6 - Colloidal Systems in Foods Containing Droplets and Bubbles. In *Understanding and Controlling the Microstructure of Complex Foods*, McClements, D. J., Ed. Woodhead Publishing: **2007**; pp 153-184.

4 D. Weaire; S. Hutzler, *The Physics of Foams*; Oxford University Press: New York, **1999**.

5 J. S. Lioumbas; E. Georgiou; M. Kostoglou; T. D. Karapantsios, Foam Free Drainage and Bubbles Size for Surfactant Concentrations Below the Cmc, *Colloids and Surfaces A: Physicochemical and Engineering Aspects* **2015**, *487*, 92-103.

6 O. Pitois; C. Fritz; M. Vignes-Adler, Liquid Drainage through Aqueous Foam: Study of the Flow on the Bubble Scale, *Journal of Colloid and Interface Science* **2005a**, *282*, 458-465.

7 O. Pitois; N. Louvet; E. Lorenceau; F. Rouyer, Node Contribution to the Permeability of Liquid Foams, *Journal of Colloid and Interface Science* **2008**, *322*, 675-677.

8 A. Anazadehsayed; N. Rezaee; J. Naser, Numerical Modelling of Flow through Foam's Node, *Journal of Colloid and Interface Science* **2017**, *504*, 485-491.

9 I. Cantat; S. Cohen-Addad; F. Elias; F. Graner; R. Höhler; O. Pitois; F. Rouyer; A. Saint-Jalmes; S. Cox, *Foams: Structure and Dynamics*; Oxford University Press: New York, **2013**.

10 C. Clarke; F. Spyropoulos; I. T. Norton, Surface Rheological Measurements of Isolated Food Foam Systems, *Physics of Fluids* **2019**, *31*, 092002.

11 M. Durand; D. Langevin, Physicochemical Approach to the Theory of Foam Drainage, *The European Physical Journal E* **2002**, *7*, 35-44.

12 A. Anazadehsayed; N. Rezaee; J. Naser; A. V. Nguyen, A Review of Aqueous Foam in Microscale, *Advances in Colloid and Interface Science* **2018**, *256*, 203-229.

13 D. Weaire; S. Hutzler; G. Verbist; E. Peters; I. Prigogine; S. A. Rice, A Review of Foam Drainage, *Advances in Chemical Physics* **1997**, *102*.

14 C. Clarke; A. Lazidis; F. Spyropoulos; I. T. Norton, Measuring the Impact of Channel Length on Liquid Flow through an Ideal Plateau Border and Node System, *Soft Matter* **2019**, *15*, 1879-1889.

15 O. Pitois; C. Fritz; M. Vignes-Adler, Hydrodynamic Resistance of a Single Foam Channel, *Colloids and Surfaces A: Physicochemical and Engineering Aspects* **2005b**, *261*, 109-114.

16 K. Koczó; G. Rácz, Flow in a Plateau Border, *Colloids and Surfaces* **1987**, *22*, 95-96.

17 F. Elias; E. Janiaud; J.-C. Bacri; B. Andreotti, Elasticity of a Soap Film Junction, *Physics of Fluids* **2014**, *26*, 037101.

18 S. Gauchet; M. Durand; D. Langevin, Foam Drainage. Possible Influence of a Non-Newtonian Surface Shear Viscosity, *Journal of Colloid and Interface Science* **2015**, *449*, 373-376.

19 K. Kinoshita; E. Parra; D. Needham, Adsorption of Ionic Surfactants at Microscopic Air-Water Interfaces Using the Micropipette Interfacial Area-Expansion Method: Measurement of the Diffusion Coefficient and Renormalization of the Mean Ionic Activity for Sds, *Journal of Colloid and Interface Science* **2017**, *504*, 765-779.

20 N. C. Christov; K. D. Danov; P. A. Kralchevsky; K. P. Ananthapadmanabhan; A. Lips, Maximum Bubble Pressure Method: Universal Surface Age and Transport Mechanisms in Surfactant Solutions, *Langmuir* **2006**, *22*, 7528-7542.

21 J. Liu; C. Yang; C. Zhang; U. Messow, Theory of Diffusion-Controlled Adsorption Kinetics at the Expanding Planar Surface with a Constant Area Rate, *Colloid and Polymer Science* **2005**, *284*, 92-96.

22 A. Bąk; W. Podgórska, Interfacial and Surface Tensions of Toluene/Water and Air/Water Systems with Nonionic Surfactants Tween 20 and Tween 80, *Colloids and Surfaces A: Physicochemical and Engineering Aspects* **2016**, *504*, 414-425.

23 O. E. Pérez; C. C. Sánchez; A. M. R. Pilosof; J. M. Rodríguez Patino, Dynamics of Adsorption of Hydroxypropyl Methylcellulose at the Air–Water Interface, *Food Hydrocolloids* **2008**, *22*, 387-402.

24 V. N. Paunov; B. P. Binks; N. P. Ashby, Adsorption of Charged Colloid Particles to Charged Liquid Surfaces, *Langmuir* **2002**, *18*, 6946-6955.

25 C. D. Dushkin; T. H. Iliev; Y. S. Radkov, Dynamic Surface Tension of Micellar Solutions Studied by the Maximum Bubble Pressure Method, *Colloid and Polymer Science* **1995**, *273*, 370-378.

26 V. B. Fainerman; V. D. Mys; A. V. Makievski; J. T. Petkov; R. Miller, Dynamic Surface Tension of Micellar Solutions in the Millisecond and Submillisecond Time Range, *Journal of Colloid and Interface Science* **2006**, *302*, 40-46.

27 B. P. Radoëv; D. S. Dimitrov; I. B. Ivanov, Hydrodynamics of Thin Liquid Films Effect of the Surfactant on the Rate of Thinning, *Colloid and Polymer Science* **1974**, *252*, 50-55.

28 I. B. Ivanov; D. S. Dimitrov, Hydrodynamics of Thin Liquid Films, *Colloid and Polymer Science* **1974**, *252*, 982-990.

29 V. G. Levich, *Physicochemical Hydrodynamics*; Longman Higher Education, **1959**, p 700.

30 L. E. Scriven; C. V. Sternling, The Marangoni Effects, *Nature* **1960**, *187*, 186-188.

31 A. Sheludko, Thin Liquid Films, *Advances in Colloid and Interface Science* **1967**, *1*, 391-464.

32 P. G. de Gennes, "Young" Soap Films, *Langmuir* **2001**, *17*, 2416-2419.

33 Chapter 6 - Transport Processes in Microfluidic Applications. In *Coulson and Richardson's Chemical Engineering (Seventh Edition)*, Chhabra, R.; Shankar, V., Eds. Butterworth-Heinemann: **2018**; pp 529-546.

34 Z. A. Zell; A. Nowbahar; V. Mansard; L. G. Leal; S. S. Deshmukh; J. M. Mecca; C. J. Tucker; T. M. Squires, Surface Shear Inviscidity of Soluble Surfactants, *Proceedings of the National Academy of Sciences* **2014**, *111*, 3677-3682.

35 V. B. Fainerman; A. V. Makievski; R. Miller, The Analysis of Dynamic Surface Tension of Sodium Alkyl Sulphate Solutions, Based on Asymptotic Equations of Adsorption Kinetic Theory, *Colloids and Surfaces A: Physicochemical and Engineering Aspects* **1994**, *87*, 61-75.

36 A. V. Nguyen, Liquid Drainage in Single Plateau Borders of Foam, *Journal of Colloid and Interface Science* **2002**, *249*, 194-199.

37 R. A. Leonard; R. Lemlich, A Study of Interstitial Liquid Flow in Foam. Part I. Theoretical Model and Application to Foam Fractionation, *AIChE Journal* **1965**, *11*, 18-25.

38 A. M. Kraynik *Foam Drainage*; United States, 1983-11-01, 1983.

39 H. Vatanparast; F. Shahabi; A. Bahramian; A. Javadi; R. Miller, The Role of Electrostatic Repulsion on Increasing Surface Activity of Anionic Surfactants in the Presence of Hydrophilic Silica Nanoparticles, *Scientific Reports* **2018**, *8*, 7251.

40 T. J. Vogel. Dynamic Behavior of Self-Assembled Langmuir Films Composed of Soluble Surfactants and Insoluble Amphiphiles. The Ohio State University, 2011.

41 A. Casandra; M.-C. Chung; B. A. Noskov; S.-Y. Lin, Adsorption Kinetics of Sodium Dodecyl Sulfate on Perturbed Air-Water Interfaces, *Colloids and Surfaces A: Physicochemical and Engineering Aspects* **2017**, *518*, 241-248.

42 K. L. Mittal, Determination of Cmc of Polysorbate 20 in Aqueous Solution by Surface Tension Method, *Journal of Pharmaceutical Sciences* **1972**, *61*, 1334-1335.

43 A. Cifuentes; J. L. Bernal; J. C. Diez-Masa, Determination of Critical Micelle Concentration Values Using Capillary Electrophoresis Instrumentation, *Analytical Chemistry* **1997**, *69*, 4271-4274.

44 S.-Y. Lin; Y.-Y. Lin; E.-M. Chen; C.-T. Hsu; C.-C. Kwan, A Study of the Equilibrium Surface Tension and the Critical Micelle Concentration of Mixed Surfactant Solutions, *Langmuir* **1999**, *15*, 4370-4376.

45 J. G. Göbel; G. R. Joppien, Dynamic Interfacial Tensions of Aqueous Triton X-100 Solutions in Contact with Air, Cyclohexane,N-Heptane, Andn-Hexadecane, *Journal of Colloid and Interface Science* **1997**, *191*, 30-37.

46 B. B. Niraula; T. K. Chun; H. Othman; M. Misran, Dynamic-Interfacial Properties of Dodecyl-B-D-Maltoside and Dodecyl-B-D-Fructofuranosyl-A-D-Glucopyranoside at Dodecane/Water Interface, *Colloids and Surfaces A: Physicochemical and Engineering Aspects* **2004**, *248*, 157-166.
47 U. Teipel; N. Aksel, Adsorption Behavior of Nonionic Surfactants Studied by Drop Volume Technique, *Chemical Engineering & Technology* **2001**, *24*, 393-400.
48 K. Staszak; K. Prochaska, Estimation of Diffusion Coefficients Based on Adsorption Measurements in Model Extraction Systems, *Chemical Engineering & Technology* **2005**, *28*, 985-990.
49 T. M. Ferreira; D. Bernin; D. Topgaard, Chapter Three - Nmr Studies of Nonionic Surfactants. In *Annual Reports on Nmr Spectroscopy*, Webb, G. A., Ed. Academic Press: **2013**; Vol. 79, pp 73-127.
50 R. D. Brazee; M. Bukovac; J. A. Cooper; H. Zhu; D. L. Reichard; R. D. Fox, Surfactant Diffusion and Dynamic Surface Tension in Spray Solutions, *Transactions of the ASAE* **1994**, *37*, 51-58.
51 Anton-Paar Viscosity of Water. https://wiki.anton-paar.com/en/water/ **2008**. (accessed 18/04/2019).
52 I. C. Bellettini; R. Eising; A. C. Felippe; J. B. Domingos; E. Minatti; V. G. Machado, Association of Branched Polyethylene Imine with Surfactants in Aqueous Solution, *Química Nova* **2015**, *38*, 787-793.
53 B. A. Kerwin, Polysorbates 20 and 80 Used in the Formulation of Protein Biotherapeutics: Structure and Degradation Pathways, *J Pharm Sci* **2008**, *97*, 2924-35.
54 M. Milanović; V. Krstonošić; L. Dokic; M. Hadnađev; T. Dapčević Hadnađev, Insight into the Interaction between Carbopol® 940 and Ionic/Nonionic Surfactant, *Journal of Surfactants and Detergents* **2015**, *18*.
55 CR *Characterization of Surfactant Mixtures*; AR204e; Krüss GmbH: 1996; p 9.
56 A. Saint-Jalmes; Y. Zhang; D. Langevin, Quantitative Description of Foam Drainage: Transitions with Surface Mobility, *Eur. Phys. J. E* **2004**, *15*, 53-60.
57 A. Saint-Jalmes, Physical Chemistry in Foam Drainage and Coarsening, *Soft Matter* **2006**, *2*, 836-849.
58 G. J. Elfring; L. G. Leal; T. M. Squires, Surface Viscosity and Marangoni Stresses at Surfactant Laden Interfaces, *Journal of Fluid Mechanics* **2016**, *792*, 712-739.

Supporting Information

A Flow Velocity Dependence of Dynamic Surface Tension in Plateau Borders of Foam

Christopher Clarke, Fotis Spyropoulos and Ian T. Norton*

*Department of Chemical Engineering, University of Birmingham, Edgbaston, Birmingham, B15 2TT, UK

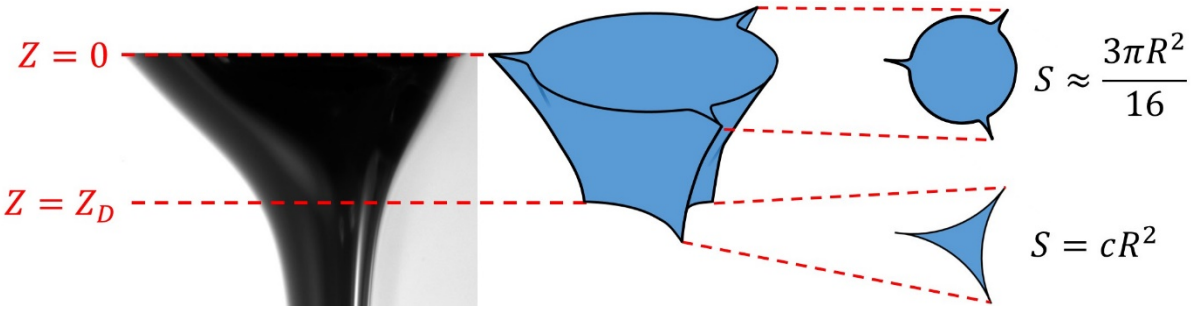

Figure S1. Characterisation of PB distortion between $Z = 0$ and $Z = Z_D$, where PB geometry transitions from an approximately circular to an ideal PB cross-section. Left – Image of PB distortion. Right – Schematics of the corresponding 2D and 3D cross-section geometries.

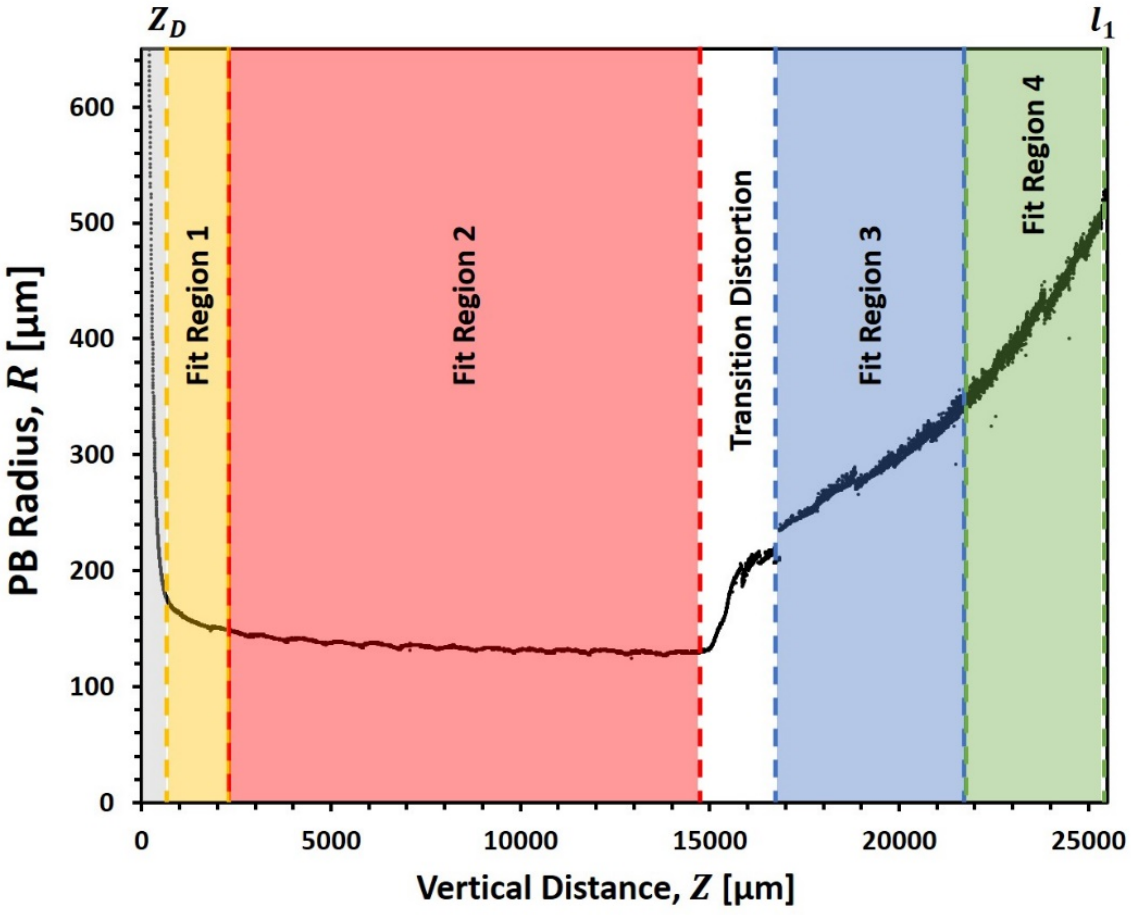

Figure S2. Example of PB profile divided into PBs fitting regions to calculate their respective surfactant residence times, τ_{Res}.

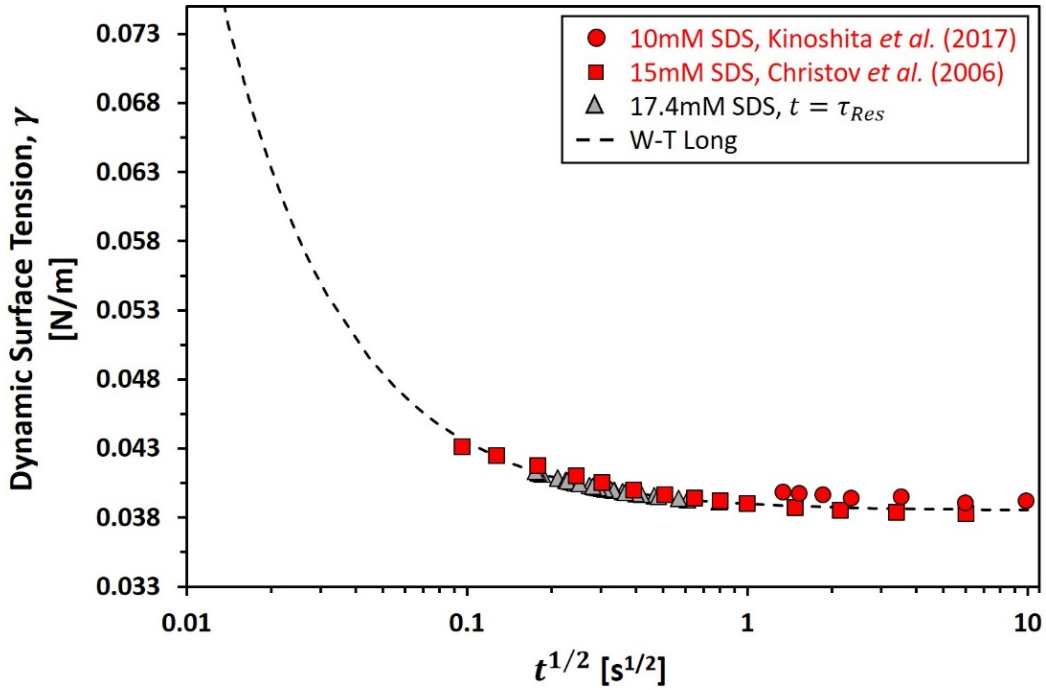

Figure S3. Comparison of calculated DST, γ, of 17.4mM SDS using the W-T long time approximation with IIA correction with $t = \tau_{Res}$, in comparison to experimental values for 10mM SDS[19] and 15mM SDS[20] from existing literature.

Derivation of Equation 1

Equation 1 describes the standard drainage theory when applied to an ideal vertical PB with liquid flow field, $\vec{u}$. An abridged version of the full derivation provided by Elias *et al.*[17] is given here in order to provide context, although it is recommended that readers refer to Elias *et al.*[17] for further detail.

Equation 1 is ultimately derived from the Navier-Stokes equation for fluid momentum (Equation S1) where P is the pressure and $\vec{f}$ is the external volume force. $\vec{f}$ itself can be described as the summation of the two forces $\overrightarrow{f_l}$ and $\overrightarrow{f_r}$ (Equation S2), where the volume force, $\overrightarrow{f_l}$, includes a 'line tension' effect due to the minimisation of PB surface energy and $\overrightarrow{f_r}$ is the elastic restoring force exerted on the PB by its three adjoining films.

$$\frac{d\vec{u}}{dt} = \vec{g} + \nu\Delta\vec{u} + \left(\vec{f} - \vec{\nabla}P\right)/\rho \tag{S1}$$

$$\vec{f} = \overrightarrow{f_l} + \overrightarrow{f_r} \tag{S2}$$

The surface free energy of the PB can be expressed as $E_s = -2\gamma l_1 cR$, where l_1 describes the length of the PB. At this point, we must also introduce a curvilinear coordinate, $\overrightarrow{s_v}$, which follows any deformation in the PB, a vector tangential to the PB, $\overrightarrow{t_v}$, and a vector normal to the PB, $\overrightarrow{n_v}$. The 'line tension', $\vec{T}$, of the PB is then expressed as:

$$\vec{T} = \frac{\partial(E_s)}{\partial l_1|_V \overrightarrow{t_v}} = -\gamma cR\overrightarrow{t_v} \tag{S3}$$

From this, we can derive the external volume force acting on the PB element between s_v and ds_v as:

$$\overrightarrow{f_l} = \left(\frac{1}{cR^2 ds_v}\right)\frac{d\vec{T}}{ds_v}ds_v = -\frac{\gamma}{R^2}\frac{dR}{ds_v}\overrightarrow{t_v} - \frac{\gamma}{R}\frac{d\overrightarrow{t_v}}{ds_v} \tag{S4}$$

Finally a force per unit length exerted by the three films is introduced in the form of Equation (S5) where $\vec{\chi}$ is a dimensionless vector and $S = cR^2$ is the PB cross-sectional area. A specific derivation of $\vec{\chi}$ can be found in Elias *et al.*[17].

$$\gamma\vec{\chi} = S\overrightarrow{f_r} \tag{S5}$$

At this point, we must also introduce the variables D and I, which are defined in Equations (6) and (7) of the main manuscript, and describe the viscous and inertial terms of the fluid flow. These were obtained by averaging across the PB horizontal cross-section[17], and can ultimately be used to describe the shape of the liquid flow velocity profiles.

$$D = -R^2\overline{\Delta u}/\bar{u} \tag{6}$$

$$I = \overline{u^2}/\bar{u}^2 \tag{7}$$

When in the steady state, substituting Equations(S4), (S5), (6) and (7) into Equation (S1) becomes:

$$I\left(\vec{\bar{u}}\cdot\vec{\nabla}\right)\vec{\bar{u}} = \vec{g} - \frac{D\nu}{R^2}\vec{\bar{u}} - \frac{\gamma}{\rho R^2}\frac{dR}{ds_v}\overrightarrow{t_v} - \frac{\gamma}{\rho R}\frac{d\overrightarrow{t_v}}{ds_v} + \frac{\gamma\vec{\chi}}{\rho cR^2} \tag{S6}$$

As $\vec{\bar{u}}$ is tangential to the PB axis, this can be rewritten as Equation S7, where the parameter, κ, is introduced to describe the curvature in the vertical plane.

$$I\left[\bar{u}^2\kappa\overrightarrow{n_v} + \bar{u}\frac{d\bar{u}}{ds_v}\overrightarrow{t_v}\right] = \vec{g} - \frac{D\nu}{R^2}\bar{u}\overrightarrow{t_v} - \frac{\gamma}{\rho R^2}\frac{dR}{ds_v}\overrightarrow{t_v} - \frac{\gamma}{\rho R}\kappa\overrightarrow{n_v} + \frac{\gamma\vec{\chi}}{\rho cR^2} \tag{S7}$$

In the ideal case of a vertical, undistorted PB, Equation S7 can be projected along the tangential vector to yield Equation 1, where the curvilinear coordinate s_v becomes equivalent to the vertical coordinate Z. Here, the definition $\bar{u} = Q/cR^2$ is used to describe the relationship between liquid flow rate and average flow velocity across the PB horizontal cross-section.

$$\frac{dR}{dZ} = \frac{cD\nu Q - gc^2R^4}{\left(\frac{2IQ^2}{R}\right) - \left(\frac{c^2R^2\gamma}{\rho}\right)} \quad (1)$$

Derivation of Equation 2

Equation (2) describes a full geometric profile solution to Equation (1) whose full derivation and explanation was conducted by Clarke *et al.*[10]. An abridged version is given here in order to provide context, although it is recommended that readers refer to Clarke *et al.*[10] for further detail.

The variables: D, ν, Q, g, c, I, γ and ρ in Equation (1) were substituted for R_e and L using Equations (4) and (5), along with an additional term, the capillary length, $L_c = \sqrt{\gamma/\rho\, g}$.

$$R_e = \left(\frac{D\nu Q}{cg}\right)^{1/4} \tag{4}$$

$$L = \frac{IQ^2}{2c^2 g {R_e}^4} - \frac{\gamma}{4\rho g R_e} \tag{5}$$

Equation (S8) sets up the solution to this revised form of Equation (1) as an integral with the limits of the initial radius, R_0, at $Z = 0$ to a radius R at a distance Z from $Z = 0$. Solving Equation (S8) yielded Equation (S9); a complete geometric PB profile solution.

$$\int_0^Z dZ = \int_{R_0}^{R} \left\{\frac{{L_c}^2}{R(R_e+R)} + \frac{{L_c}^2 R_e}{({R_e}^2+R^2)(R_e+R)} + \frac{4L{R_e}^4}{R({R_e}^4-R^4)}\right\} \cdot dR \tag{S8}$$

$$Z = L\, ln\left[\frac{R^4({R_0}^4-{R_e}^4)}{{R_0}^4(R^4-{R_e}^4)}\right] + \frac{{L_c}^2}{4R_e}\left\{ln\left[\frac{R^4(R_0+R_e)^2({R_0}^2+{R_e}^2)}{{R_0}^4(R+R_e)^2(R^2+{R_e}^2)}\right] + 2\, tan^{-1}\left[\frac{R-R_0}{R_e(1+RR_0/{R_e}^2)}\right]\right\} \tag{S9}$$

The minimum of Equation (S9) can be found at the coordinates $[Z = 0, R = R_0]$ where R_0 is described by Equation (3) in the main manuscript.

Clarke *et al.*[10] subsequently demonstrated that the unusual shapes of PB profiles observed during their experiments could be explained by the presence a zero offset, Z_T, to Equation (S9), which resulted from the geometry of the adjoining node at $[Z = l_1, R = R_{n0}]$. The inclusion of the offset yielded Equation (2).